



Exploring the dynamics of the ABCB1 membrane transporter P-glycoprotein in the presence of ATP and active/non-active compounds through molecular dynamics simulations

Liadys Mora Lagares^{a,*}, Yunierkis Pérez-Castillo^b, Marjana Novič^{a,*}

^a Theory Department, Laboratory for Cheminformatics, National Institute of Chemistry, 1000 Ljubljana, Slovenia

^b Bio-Cheminformatics Research Group and Escuela de Ciencias Físicas y Matemáticas, Universidad de Las Américas, Quito 170513, Ecuador

ARTICLE INFO

Handling Editor: Dr. Mathieu Vinken

Keywords:

P-glycoprotein
In silico
Molecular dynamics simulations
ABC transporter
Conformational changes, ATP

ABSTRACT

P-glycoprotein (Pgp) is a member of the ATP-binding cassette family of transporters that confers multidrug resistance to cancer cells and is actively involved in the pharmacokinetics and toxicokinetics of a big variety of drugs. Extensive studies have provided insights into the binding of many compounds, but the precise mechanism of translocation across the membrane remains unknown; in this context, the major challenge has been to understand the basis for its polyspecificity. In this study, molecular dynamics (MD) simulations of human P-gp (hP-gp) in an explicit membrane-and-water environment were performed to investigate the dynamic behavior of the transporter in the presence of different compounds (active and inactive) in the binding pocket and ATP molecules within the nucleotide binding domains (NBDs). The complexes studied involve four compounds: cyclosporin A (CSA), amiodarone (AMI), pamidronate (APD), and valproic acid (VPA). While CSA and AMI are known to interact with P-gp, APD and VPA do not. The results highlighted how the presence of ATP notably contributed to increased flexibility of key residues in NBD1 of active systems, indicating potential conformational changes activating the translocation mechanism. MD simulations reveal how these domains adapt and respond to the presence of different substrates, as well as the influence of ATP binding on their flexibility. Furthermore, distinctive behavior was observed in the presence of active and inactive compounds, particularly in the arrangement of ATP between NBDs, supporting the proposed nucleotide sandwich dimer mechanism for ATP binding. This study provides comprehensive insights into P-gp behavior with various ligands and ATP, offering implications for drug development, toxicity assessment and demonstrating the validity of the results derived from the MD simulations.

1. Introduction

P-glycoprotein, also known as P-gp or ABCB1, is an important membrane protein belonging to the ATP-binding cassette (ABC) transporter superfamily (Li et al., 2010). Its primary function is to serve as a guardian in cellular defense mechanisms, protecting tissues from potentially harmful substances, including pharmaceutical compounds. P-gp is abundantly expressed in a variety of cells and tissues, such as those forming the gastrointestinal tract, liver, kidney, and blood-brain barrier (Sharom, 2008). This widespread distribution highlights its important role influencing the pharmacokinetics and toxicokinetics of various therapeutic agents.

Discovered in the late 1970 s (Juliano and Ling, 1976), P-gp's

primary function is efflux transport. It actively expels a diverse range of substrates from within cells to the extracellular environment. This action diminishes the intracellular levels of potentially toxic compounds, preventing their detrimental effects. Therefore, P-gp significantly impacts the processes of absorption, distribution, metabolism, excretion, and toxicity (ADMET) (Li et al., 2014) of numerous drugs, thereby playing a crucial role in their overall disposition.

P-gp has a versatile substrate specificity, encompassing a wide array of structurally diverse molecules, such as chemotherapeutic drugs, antibiotics, antivirals, immunosuppressants, and many more. This broad specificity, combined with its prevalence in crucial tissues, positions P-gp as a significant contributor to the phenomenon of multidrug resistance (MDR) (Ambudkar et al., 2003; Leslie et al., 2005) observed in

* Corresponding authors.

E-mail addresses: liadys.moralagares@ki.si (L. Mora Lagares), marjana.novic@ki.si (M. Novič).

<https://doi.org/10.1016/j.tox.2024.153732>

Received 20 December 2023; Received in revised form 15 January 2024; Accepted 17 January 2024

Available online 24 January 2024

0300-483X/© 2024 The Author(s). Published by Elsevier B.V. This is an open access article under the CC BY license (<http://creativecommons.org/licenses/by/4.0/>).

various cancers and infectious diseases, where cells develop resistance to a variety of structurally and functionally unrelated chemotherapeutic agents.

P-gp is a large membrane protein, with a structure consisting of 1280 amino acids organized into two symmetrical halves, each containing six transmembrane helices connected by cytosolic loops, and two cytosolic ATP binding regions known as nucleotide binding domains (NBDs) (Fig. 1). The transmembrane domains (TMDs) take on the responsibility of facilitating substrate translocation across the membrane (Zhou, 2008). Meanwhile, each NBD contains conserved sequence motifs essential for ATP binding, known as the Walker A and Walker B motifs, as well as the ABC signature motif. Upon ATP binding, the NBDs come together, enabling ATP hydrolysis. This event provides the energy required for conformational changes in the transmembrane domains, ultimately driving substrate translocation across the membrane.

It is noteworthy that the effective nucleotide binding site is only formed when the NBDs dimerize, consisting of the Walker A motif of one NBD and the ABC motif of the other NBD. A Mg^{2+} ion, vital for ATP hydrolysis, binds to the Walker B motif (Chen et al., 2003; Smith et al., 2002).

Moreover, the ATP binding site plays a crucial role in stabilizing the conformation of P-glycoprotein (Dehghani-Ghahnaviyeh et al., 2021; Lusvarghi and Ambudkar, 2019; Pan and Aller, 2015), particularly in the closed conformation associated with substrate transport, as ATP molecules stabilize a sandwich-like conformation between the two NBDs, preserving the dimensions of the drug-binding pocket (Smith et al., 2002).

P-gp undergoes conformational changes, transitioning from an inward-facing state, open to the cytoplasm, to an outward-facing state, open to the extracellular space. In its inward-facing conformation, P-gp exhibits a strong affinity for substrate binding, effectively capturing molecules from the intracellular compartment or the lipid bilayer of the plasma membrane. This conformation is crucial for substrate recognition and initial binding. On the other hand, in the outward-facing conformation, P-gp expels the bound substrates into the extracellular space. This transition involves large structural rearrangements, including the movement of TMDs and NBDs. The functional interplay between these distinct conformations is essential for P-gp's role as an efflux pump.

Gaining a deep comprehension of the intricate mechanism underlying of P-gp has emerged as a critical area of research, with implications for refining drug treatment protocols, overcoming MDR and designing novel compounds with enhanced pharmacokinetic and toxicokinetic profiles. In this context, molecular dynamics (MD) simulations have emerged as a powerful tool for elucidating the dynamic behaviors of proteins, including transporters like P-gp (Condic-Jurkic et al., 2018). MD simulations enable researchers to observe the molecular-level interactions between diverse compounds and P-gp. This includes exploration of the binding pockets, identification of key residues involved in substrate recognition, and understanding of the factors influencing substrate selectivity (Mora Lagares et al., 2021).

MD simulations have proven to be a valuable tool in hazard assessment, offering new insights into the dynamic behavior of molecules at the atomic level. They have significantly contributed to improve our

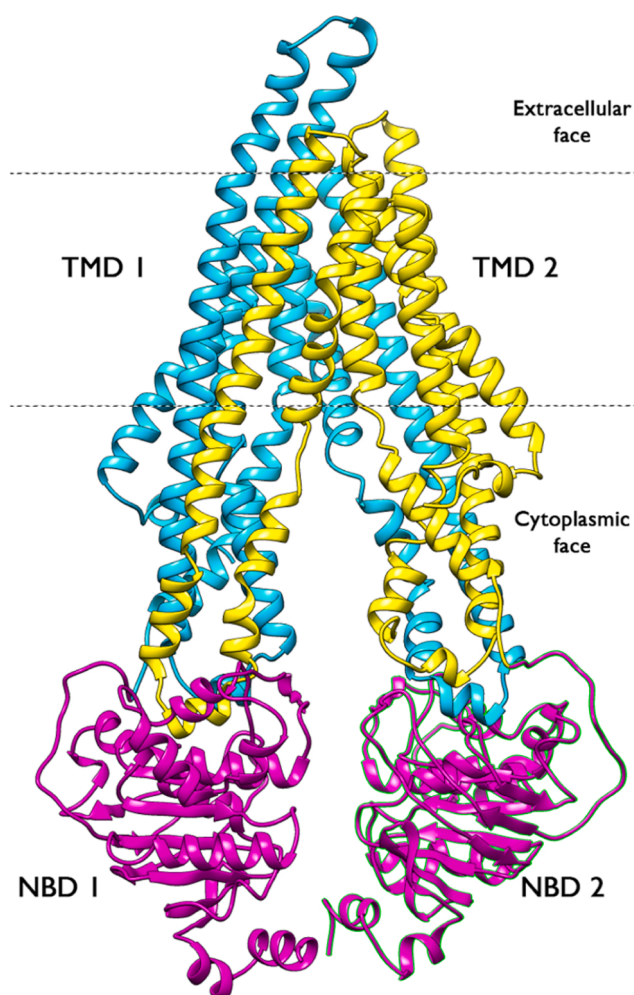


Fig. 1. Cryo-EM structures of hP-gp in the inward facing conformation (PDB ID: 6QEX). NBDs are shown in magenta and TMDs are shown in cyan and yellow.

ability assessing the potential hazards associated with various compounds, facilitating a comprehensive understanding of how chemicals interact with biological systems, a critical factor in assessing the potential toxicity and adverse effects of substances, thereby supporting the development of safer alternatives.

The integration of MD simulations with other *in silico* approaches, such as Quantitative Structure-Activity Relationship (QSAR) models and structure-based predictions, offers a comprehensive framework for hazard assessment. This collaborative approach relies on the strengths of each method, leading to more accurate and reliable predictions. As these methodologies continue to evolve, they show great promise in transforming the way we approach and address safety concerns in various fields, from pharmaceuticals to environmental protection. It would contribute to the so called “New Approach Methodologies” (NAMs), which aim to protect human health when integrated into the risk assessment of chemical, and can be further developed into an animal-free “Next Generation Risk Assessment” (Schmeisser et al., 2023).

In this context, MD simulations have already been used to study P-gp drug interactions and other dynamic processes of P-gp (Ferreira et al., 2012; Grigoreva et al., 2022; O'Mara and Mark, 2012; Zhang et al., 2021). Nevertheless, due to the unavailability of the human crystal structure of P-gp (*hP-gp*) at the time, the reported studies were performed either on homology models or on the crystal structure of mouse P-gp (*mP-gp*). Notably, in 2019, the cryo-electron microscopy (cryoEM) structure of *hP-gp* in the inward facing conformation was solved (PDB ID: 6QEX) (Alam et al., 2019), and some studies have emerged utilizing this updated structural data (Mora Lagares et al., 2021).

Understanding the dynamic behavior of P-gp seems essential due to its functional significance, physiological distribution, substrate specificity, and its profound impact on drug development and toxicity assessment. It would contribute to the mechanistic interpretation of data-driven models for prediction of potential interactions of any compounds with P-gp. Here, we describe a series of MD simulations based on the human cryo-EM structure of P-gp and the presence of ATP molecules. Our objective is to analyze the behavior of the transporter in the presence of different molecules (both active and inactive compounds) within the binding pocket, while also evaluating how nucleotide binding influence the dynamics of the nucleotide-binding domains (NBDs) and transmembrane domains (TMDs). Through this approach, we aim to identify movement patterns that contribute to the initial steps of the efflux mechanism, and also to pinpoint other characteristics that would allow us to distinguish between active and inactive compounds.

2. Materials and Methods

2.1. Preparation of the initial structures

The initial structure of P-gp used for the simulations corresponds to the cryoEM structure of the *hP-gp* (PDB ID: 6QEX) (Alam et al., 2019). The initial setup for the molecular dynamics simulations involving the ligand-P-gp complexes was derived from prior docking calculations as outlined in (Mora Lagares et al., 2020). The ATP molecule coordinates were sourced from the cryoEM structure of the *hP-gp* (PDB ID: 6COV) (Kim and Chen, 2018).

The initial complexes were built and parameterized using the CHARMM-GUI web-based graphical user interface (Jo et al., 2014, 2008; Lee et al., 2020). The force fields employed included FF19SB for the protein, LIPID17 for the lipids and GAFF2 for the ligands. The fast semiempirical method of Austin Model 1 with bond charge corrections (AM1-BCC) was used to generate atomic charges for the ligands (He et al., 2020). The ligand-P-gp complex was solvated using the TIP3P explicit water model. The system was then embedded into a lipid membrane formed by 1-palmitoyl-2-oleoyl-phosphatidylcholine (POPC), 1-Palmitoyl-2-oleoyl-sn-glycero-3-phosphoethanolamine (POPE) and Cholesterol (CHL) in a ratio of 2:2:1. The protein-ligand complex was placed in the center of the lipid bilayer, with its long

axis perpendicular to the lipid surface. To keep the system neutrality, potassium (K^+) and chloride (Cl^-) ions were added at a concentration of 0.15 M.

2.2. Molecular dynamics simulations

The MD simulations were performed using Amber 2018 software (Case et al., 2018).

2.2.1. Simulation parameters

Periodic boundary conditions (PBC) were implemented in all simulations. Bonds involving hydrogen atoms were constrained through the SHAKE algorithm. Long-range electrostatic interactions were computed using the Particle-Mesh Ewald (PME) method, with a non-bonded cutoff radius of 10 Å for the van der Waals and electrostatic interactions. The system temperature was stabilized at 303 K using a Langevin thermostat with a collision frequency of 1.0 ps^{-1} . In the NPT runs, pressure was regulated to 1 bar using the Berendsen barostat. The system pressure was semiisotropically coupled, meaning it was balanced by separately coupling the lateral (x and y) and normal (z) box directions. The energy minimization and equilibration stages were performed following the CHARMM-GUI provided files as described below. The trajectory analyses were performed using the CPPTRAJ (Roe et al., 2013) module of AmberTools (Case et al., 2018), VMD (Humphrey et al., 1996), UCSF Chimera (Pettersen et al., 2004), MDtraj (McGibbon et al., 2015), and POVME 3.0 (Wagner et al., 2017).

2.2.2. Energy minimization

The energy minimization run consisted in 2500 steps of steepest descent method, followed by 2500 cycles of conjugate gradient. The entire system was restrained with a force constant of $10 \text{ kcal/mol } \text{Å}^2$, allowing only the water molecules to move freely.

2.2.3. Equilibration

The equilibration phase was carried out in several steps. Initially, three consecutive NVT simulations of 125 ps each were conducted with restraints applied to the protein, ligand, and lipid head groups of the membrane. The maximum restraint force applied to the protein and ligands was $10 \text{ kcal/mol } \text{Å}^2$, and to the membrane was $2.5 \text{ kcal/mol } \text{Å}^2$. Subsequently, three consecutive NPT runs of 500 ps were performed to gradually remove the restraints on the system. The time step was set at 2 fs. This equilibrated system served as the starting point for the 500 ns completely unrestrained NPT production run.

2.2.4. Production

The production phase was performed in the NTP ensemble at a temperature of 303 K and 1 bar pressure. The time step was established at 2 fs, with trajectory snapshots saved every 50,000 steps (equivalent to 100 ps). Two replica simulations were carried out for the ligand-P-gp complexes, each of 500 ns. This accounted for a total simulation time of 4 μs .

2.3. Trajectory analysis

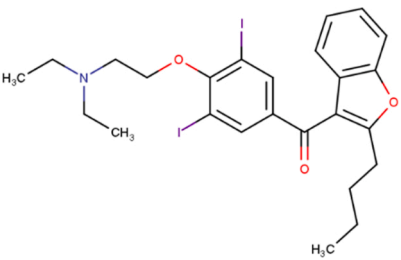
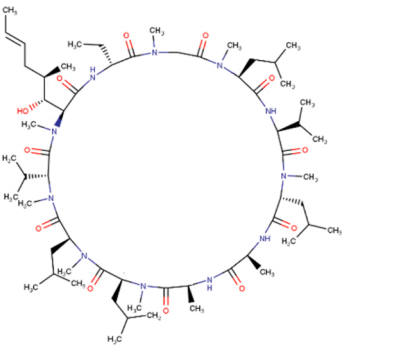
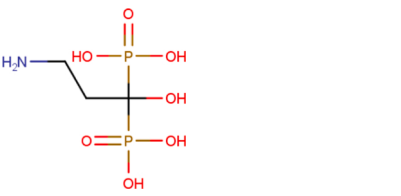
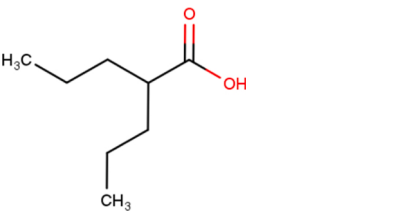
To assess the average deviations in atomic positions and the stability of the MD trajectories, the atomic root-mean-square deviations (RMSD) for each system were computed using the CPPTRAJ module (Roe et al., 2013) of the AmberTools package (Case et al., 2018). During RMSD calculation, every frame of the trajectory was aligned to minimize the RMSD between the protein backbone at the given frame and the reference initial structure, corresponding to the resulting structure after minimization.

2.3.1. Principal component analysis

A principal component analysis (PCA) was performed to analyze the conformational changes and primary modes of motion exhibited by P-gp

Table 1

. 2D structures of the molecules used in the study.

Name	Chemical structure
Amiodarone	
Cyclosporine A	
Pamidronate	
Valproic acid	

throughout the 500 ns production runs. PCA is a technique employed to transform a potentially correlated set of observations into a set of orthogonal vectors, known as principal components (PCs). These PCs explain the variance in the data, with the first PC carrying the largest variance, the second PC the next largest, and so on.

The input to the PCA consisted of the covariance matrix derived from the time series of position coordinates. Consequently, the PCs represent distinct modes of motion for the system, with the first PC delineating the dominant motion. This matrix comprises covariance values between the X, Y, and Z components of each atom, resulting in a final matrix size of $3N \times 3N$, where N is the number of atoms. Given our focus on the

internal dynamics of the system, rotational and translational movements were eliminated by conducting a coordinate RMS fit to a reference structure, specifically, the *hP-gp* cryoEM structure. Following the removal of all translations and rotations, the covariance matrix was constructed based on the C α coordinates.

The covariance matrix was then diagonalized to obtain the eigenvectors (PCs) and the eigenvalues (representing the weight of each PC) that characterize the primary modes of structural variation. Through this process, an orthogonal set of unitary vectors emerged, defining the directions of maximum variation within the observed conformational distribution. Each eigenvector is linked to an eigenvalue, which dictates

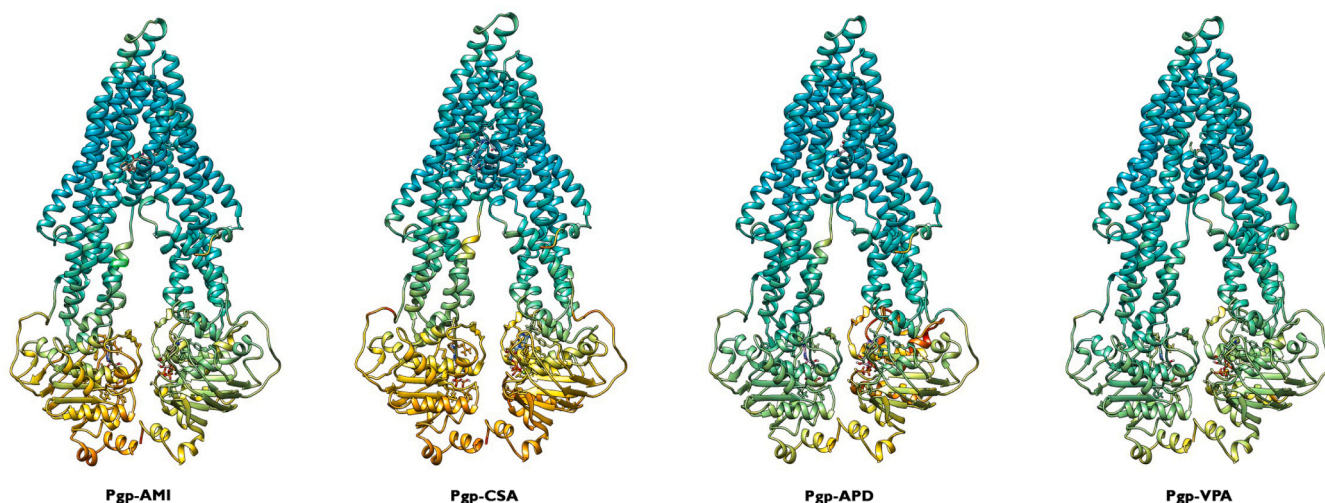


Fig. 2. Colored representation of Root-Mean-Square Fluctuations (RMSF) for the simulated P-glycoprotein (P-gp)-ligand systems during the 500 ns production run. The color spectrum represents flexibility, ranging from cyan (indicating lower values) to red (indicating higher values). Consistently, the same regions exhibit high flexibility across all studied systems. Notably, flexibility is more pronounced in the active complexes. The four ligands studied are AMI, CSA, APD, and VPA, with the latter two known not to interact with P-gp.

the magnitude of movements along its corresponding principal axis. The sum of all eigenvalues collectively accounts for the total conformational variance of the system. The relative contribution of each eigenvector to the overall system flexibility is calculated as the ratio between its associated eigenvalue and the total system flexibility. While PCA provides valuable insights into system dynamics, it's important to note that the actual motion observed in a simulation typically involves a combination of individual PCs.

The PCA analysis was conducted using the CPPTRAJ module (Roe et al., 2013) within the AmberTools package (Case et al., 2018). The visualization of principal component data was carried out using the Normal Mode Wizard (NMwiz) plugin (Bakan et al., 2011) for VMD.

2.3.2. Nucleotide binding domains (NBDs) cavity volume

The calculation of NBDs cavity volumes was conducted using the tool Pocket Volume Measurer POVME 3.0 (Wagner et al., 2017). The POVME algorithm determines the pocket volume by subtracting the volume occupied by the protein atoms in each frame from the specified inclusion region, which sets the boundaries of the pocket. The assessment of the NBDs cavity volume for each system was carried out using as input PDB trajectories containing 100 frames extracted from each respective production trajectory. The pocket inclusion region was ligand-defined, meaning it encompassed all grid points within 3 Å of the ligand atoms in the loaded PDB trajectory.

To identify representative binding pocket conformations, and to determine the average pocket shape in each group of systems, a pocket shape clustering procedure was carried out. To facilitate this, the ligands were extracted from the trajectories, and they were combined to generate two new sets of trajectories: one containing the merged trajectories of the active systems, and the other with the combined trajectories of the inactive systems. These trajectories were then aligned, and the inclusion region was defined utilizing the ATP residue name to define the location of the binding cavity. The resulting average pocket shape of each group was then visualized in VMD (Humphrey et al., 1996).

2.3.3. Solvent-accessible surface area (SASA)

The overall Solvent Accessible Surface Area (SASA) was calculated from the 500 ns production trajectories of each system using the Surf action command within the CPPTRAJ module (Roe et al., 2013) in the AmberTools package (Case et al., 2018). This command employs the Linear Combinations of Pairwise Overlaps (LCPO) algorithm (Weiser et al., 1999) to compute the surface area in square angstroms (Å²). In contrast, the per-residue SASA was computed using the Python library MDtraj (McGibbon et al., 2015).

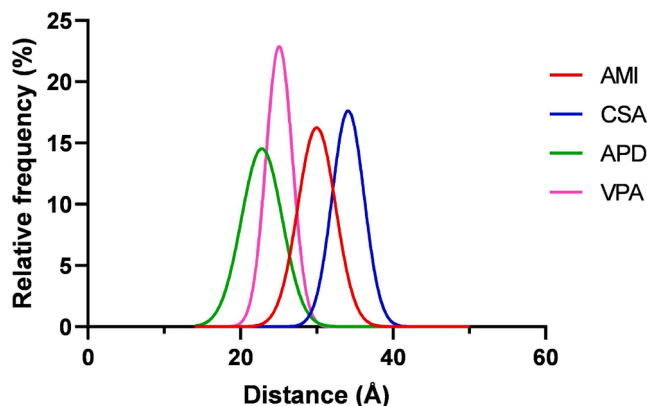


Fig. 3. Distance distribution curves between the NBDs across the simulation time for all the examined systems.

Table 2

PCA results for the 500 ns simulation run of P-gp ligand-bound systems.

Eigenvector	Cumulated eigenvalues expressed in percent (%) ¹			
	Pgp-AMI	Pgp-CSA	Pgp-APD	Pgp-VPA
1	39.69	58.61	50.04	35.56
2	54.72	75.52	66.58	55.87
3	67.71	80.72	76.93	68.95
4	77.67	83.67	83.98	74.45
5	82.44	85.84	86.45	78.27
6	84.56	87.59	88.19	80.48
7	86.57	88.69	89.16	82.25
8	87.86	89.67	89.96	83.80
9	88.99	90.54	90.63	85.03
10	90.07	91.21	91.24	85.97

¹Flexibility explained by eigenvectors from 1 to n.

3. Results

Molecular dynamics simulations were performed on a set of ligand–P-gp complexes involving four distinct compounds (see Table 1). This collection comprised two drugs recognized for their interaction with P-gp as substrates or inhibitors: cyclosporin A (CSA), a high-affinity substrate (Mora Lagares et al., 2020; Saeki et al., 1993) and inhibitor (Mora Lagares et al., 2020; Wigler, 1999) of P-gp; amiodarone (AMI) (Mora Lagares et al., 2020; Jouan et al., 2016); and two compounds that do not interact with P-gp: pamidronate (APD) (Mora Lagares et al., 2020), and valproic acid (VPA) (Mora Lagares et al., 2020; Baltes et al., 2007; Eyal et al., 2006; Yang et al., 2008). This approach represents a novel contribution, as previous studies primarily relied on the structure of mP-gp or homology models of hP-gp. Additionally, we introduced a novel aspect to our simulations by including the ATP molecules, further enhancing the comprehensiveness of our investigation.

3.1. Molecular dynamics characterization of P-gp systems

The root mean square deviation (RMSD) results showed that the P-gp-ligand complexes were stabilized after 50 ns because the fluctuation was minimal and ranged within 3 Å (Supplementary Materials Fig. S1). For P-gp active ligands, low RMSD values indicate stable complexes with minimal fluctuations (~1 Å), while non-active compounds display larger and more consistent fluctuations during simulation, suggesting less stable binding.

The root-mean-square fluctuations (RMSF) were consistent across all systems, with residue fluctuations generally staying below 3 Å,

compared to the mean structure. Significant fluctuations were observed in loop regions and NBDs, while transmembrane helices remained stable (Supplementary Materials Fig. S2). Particularly of interest, NBD fluctuations exhibited reduced intensity in the presence of ATP molecules, in contrast to our previous study conducted without nucleotides (Supplementary Materials Fig. S4) (Mora Lagares et al., 2021). However, the flexibility of all the systems is still mostly localized at the NBDs region. Remarkably, active complexes displayed higher flexibility compared to their inactive counterparts (Fig. 2). This outcome is in line with expectations, as the activation of the translocation pathway, a process associated with active ligands, needs increased movement in both NBDs. Additionally, the RMSF of the ligands alone was also analyzed, and as anticipated, the active ones exhibited lower fluctuation (i.e., greater stability) compared to the inactive ones (see Supplementary Materials Table S1).

The gap between NBDs was closely tracked during the simulation time, specifically measuring the distance between the backbone nitrogen in the Lysine residue within the Walker A motif in NBD1, and the C α atom of the Serine residue within the signature motif of NBD2. These are conserved motifs which play a crucial role in ATP binding and hydrolysis (Domicevica and Biggin, 2015). In active systems, the most frequent distances exceeded 30 Å, whereas in inactive systems, they were below 30 Å (Supplementary Materials Fig. S3). Examination of the distance distribution curves (Fig. 3, Supplementary Materials Fig. S5) showed a noticeable difference compared to the study conducted without ATP (Mora Lagares et al., 2021). Notably, the distributions were narrower in the presence of ATP, suggesting that the NBDs remained in closer proximity with the presence of the nucleotides.

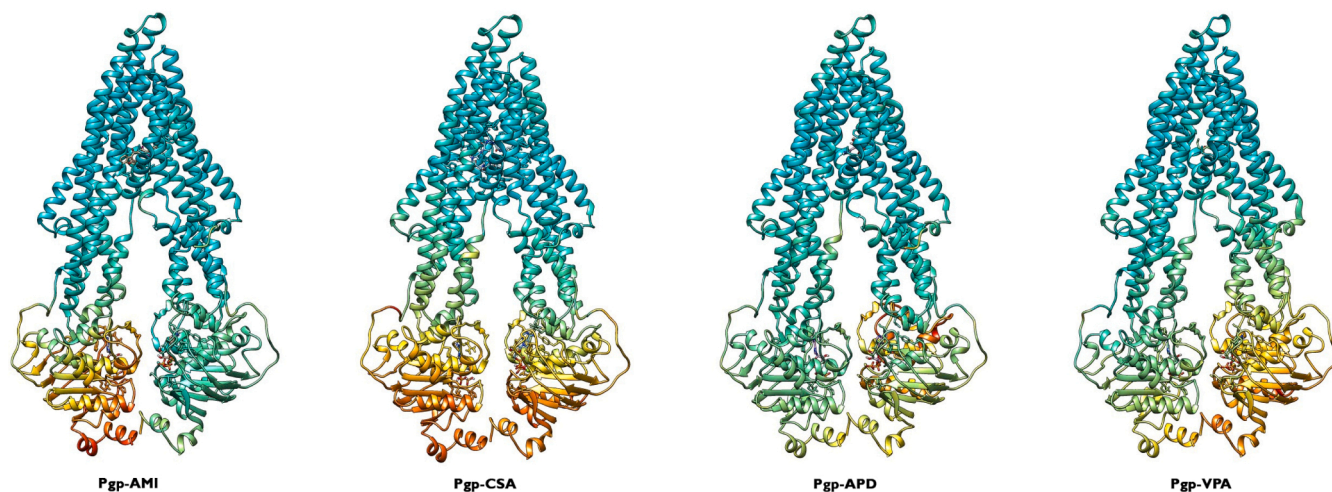


Fig. 4. Colored representation of Root-Mean-Square Fluctuations (RMSF) for the simulated P-glycoprotein (P-gp)-ligand systems along the first principal component (PC1) during the 500 ns production run. The color spectrum represents flexibility, ranging from cyan (indicating lower values) to red (indicating higher values). Consistently, the same regions exhibit high flexibility across all studied systems. Notably, flexibility is more pronounced in the active complexes.

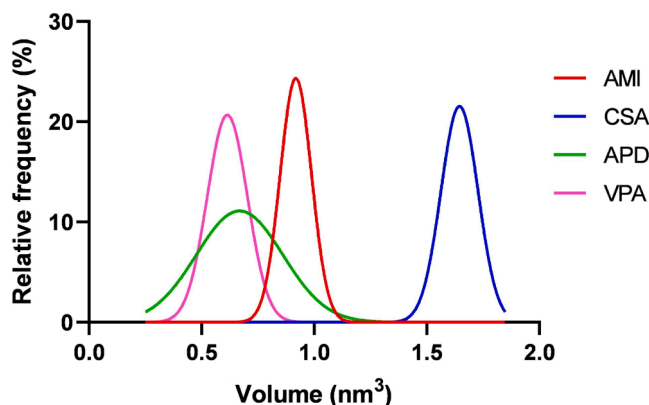


Fig. 5. Distributions of the binding pocket volumes.

3.2. Role of the nucleotides in the conformational changes of P-gp systems

Principal Components Analysis (PCA) was used to identify the conformational changes and primary modes of motion exhibited by P-gp throughout the simulation period. PC1 and PC2, the first two principal axes, together explain between 54.72% and 75.52% of the total system motion (Table 2). Subsequently, the trajectories were projected onto PC1, which captures the highest structural variability along the trajectory.

Along the first principal component, the RMSF analysis (Fig. 4) showed predominant conformational changes occurring in NBD1 for the active systems. In P-gp–CSA complex, both NBDs demonstrated a high degree of flexibility. In the inactive systems, the conformational changes were less extensive and more evenly distributed between both NBDs, e.g., P-gp–APD complex. Similarly, as observed in the study without ATP (Mora Lagares et al., 2021), the NBD2 displayed the highest degree of flexibility in the P-gp–VPA complex. This behaviour could be related to the additional property of VPA of influencing the expression and function of P-gp as documented in the studies by Eyal et al. and Yang et al (Eyal et al., 2006; Yang et al., 2008). Therefore, its inductive nature could be the reason for the observed differences in movement patterns, which were not entirely consistent with observations for strictly active or inactive compounds.

However, when examining the individual atomic fluctuation values along PC1, it was observed that the residues in NBD1 exhibit higher fluctuations in the active systems. This increase in flexibility reaches up to 276.89% when compared to the inactive complexes. For example, the residues of the ABC signature motif in NBD1 have higher fluctuations compared to any of the inactive systems, with flexibility increases ranging from 176.20% to 191.93%, and the walker A motif ranging from 85.34% to 209.48%. The presence of ATP notably contributed to the

enhanced flexibility of key residues in NBD1, suggesting a dynamic leading to the activation of the translocation mechanism, as the ATP binding site is formed by the Walker A motif of one NBD and the signature motif of the other NBD.

The PCA results were also used to identify and visualize the primary motion patterns of the protein. Along PC1, the predominant structural variability in the transporter when an active compound is present, involves the motion of NBD1 and NBD2 drawing closer. While the specific nature of this motion differs in each system (see Supplementary Materials Fig. S6), the ABC motif in NBD1 and the Walker A motif in NBD2 tend to approach as the NBDs undergo movement. This is a significant observation, since the ATP binding site is formed between these two conserved motifs as mentioned in the previous paragraph.

3.3. Binding pocket volume

The volume of the binding pocket remained largely consistent compared to the previous study (Mora Lagares et al., 2021). There are no significant differences or patterns in the volume distribution curves between active and inactive systems (Fig. 5, Supplementary Materials Fig. S7). It is worth noting that the inactive compounds, despite being the smallest in the group, do not induce conformational changes that would reduce the volume of the binding pocket. CSA, being the largest molecule in the set, shows the broadest distribution, emphasizing the binding pocket's ability to accommodate a range of ligand sizes.

3.4. Nucleotide binding domains (NBDs) cavity volume

During the simulations, it was also monitored the volume of the cavity located between the NBDs, which serves to accommodate the

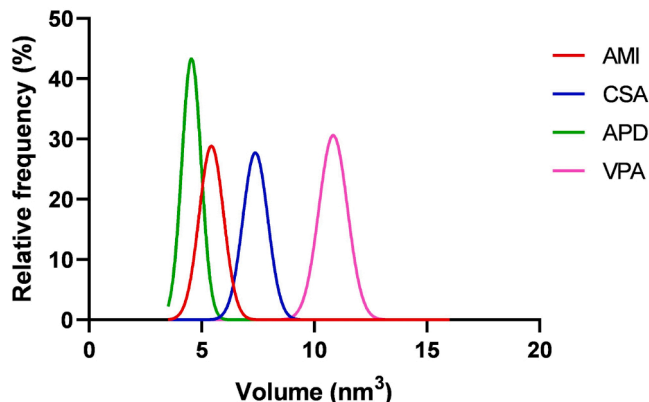


Fig. 6. Distributions of the NBDs pocket volumes.

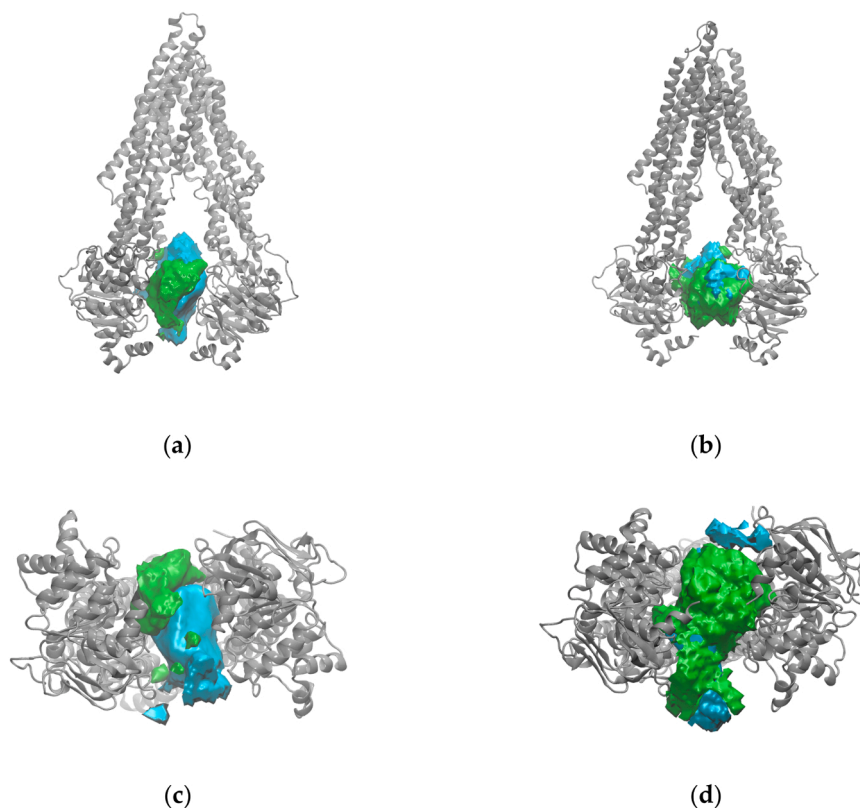


Fig. 7. Average ATP binding pocket shape for the most populated cluster: **(a)** Front view of active systems; **(b)** Front view of inactive systems; **(c)** Lower view of active systems; **(d)** Lower view of Inactive systems. The blue surface represents the average pocket shape. Additionally, the areas exhibiting greater openness compared to the average shape are illustrated with a green surface.

nucleotide molecules (ATP binding cavity). As illustrated in the distribution curves in Fig. 6, and Supplementary Materials Fig. S8, the active systems consistently maintain similar volumes over the course of the simulation. In contrast, the inactive complexes display a significant difference in volume sizes.

The average shape of the cavity was examined through a clustering analysis of the ATP binding cavities. This analysis was performed separately for the combined trajectories of active and inactive systems. Each analyzed frame was categorized into a single cluster, representing frequently visited pocket shapes (see, Supplementary Materials Fig. S9). From each system, five clusters were generated. It is important to note that the average pocket size was larger in the active systems, with an average volume of 15764.24 \AA^3 , compared to 11475.47 \AA^3 in the inactive systems. However, in the inactive systems, the clusters explored areas outside the average pocket more extensively, indicating less stable binding, as depicted in Fig. 7, where the green areas indicate regions that are more open compared to the average shape. It is anticipated that in active systems, where the binding of ATP to the NBDs is crucial, the nucleotides should explore a more restricted region compared to systems where binding is not expected. This implies the presence of more specific interactions and less flexibility of ATP in active systems.

3.5. A key distinction between active and inactive systems

An observed, remarkable difference between active and inactive systems lies in the arrangement of ATP molecules between the NBDs. In the active systems, the nucleotides tend to cluster, bringing their surfaces into close contact. Conversely, in inactive complexes, they remain separated (see Fig. 8). These observations support the ATP binding mechanism called “nucleotide sandwich dimer”, first proposed by Jones et al (Jones and George, 1999, 2002), in which ATP stabilizes a sandwich-like conformation formed by the two NBDs with a layer of two

ATP molecules. In this state, the transporter retains the ability to capture substrates while preserving the dimensions of the drug binding pocket. Dimerization of the NBDs is fundamental to the catalytic cycle of the ABC transporter by coupling with rearrangements in the TMDs and subsequent transport of the substrate across the membrane; therefore, both NBDs are essential for the correct function of P gp. It is likely that P-gp primarily adopts this configuration in cellular environments, where there is an abundance of available ATP (Grigoreva et al., 2022).

3.6. Exposure of surfaces to the solvent

Comparing the solvent-accessible surface area (SASA) graphs (Fig. 9) with those reported in our previous work (Mora Lagares et al., 2021), there is an approximate reduction of 100 nm^2 ($\approx 15\%$) which could be attributed to the presence of ATP, which renders the interacting residues less accessible.

The presence of ATP led to reduced SASA values of certain residues within the NBDs as depicted in Fig. 10, compared to the previous simulations conducted without nucleotides. On the other hand, some residues in the extracellular loops, crucial for allowing a rapid closure of the outward-facing conformation, thus preventing substrate re-entry into the translocation pathway (Kim and Chen, 2018), displayed an increased flexibility, indicated by larger SASA values. Furthermore, it was observed that in the active systems, residues from the flexible loops interrupting TM4 and TM10 in the inward-facing conformation displayed larger SASA values, a phenomenon not observed in the study conducted without ATP. This observation is consistent with existing literature suggesting that these loops function as flexible hinges for opening the drug-translocation pathway (Jin et al., 2012; Kodan et al., 2014).

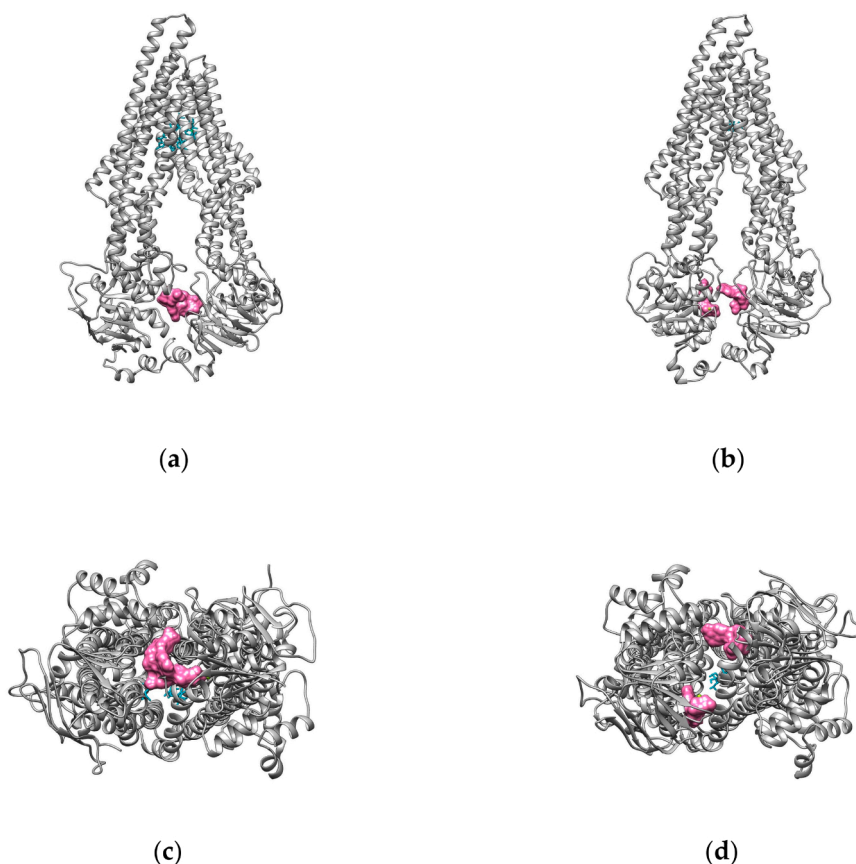


Fig. 8. Surface Representation of ATP in the NBDs Pocket: (a) Front view of active systems; (b) Front view of inactive systems; (c) Lower view of active systems; (d) Lower view of Inactive systems. The ATP molecules are represented with a pink surface.

4. Conclusions

In this study, molecular dynamics simulations were conducted on a range of ligand-P-gp complexes, including active and inactive compounds. The approach incorporated ATP molecules into the simulations, further enhancing the depth of the investigation.

The study revealed notable differences between both types of system. Firstly, there was a general increase in flexibility in NBD1 with respect to the rest of the protein, especially pronounced in the active systems, as demonstrated by the PCA results. The higher fluctuations in NBD1 emerged as a distinctive feature for their differentiation.

Moreover, the simulations unveiled distinct characteristics regarding ATP molecules in the NBDs. In active systems, the nucleotides remained in close contact along the simulation time, whereas in inactive systems,

they kept a noticeable distance from each other. This observation holds potential for predicting a compound's interaction with the transporter. On the other hand, the PCA analysis was also helpful in detecting motion patterns characterized by the two cytosolic NBDs making extensive contacts with each other forming the typical "head-to-tail" dimer characteristic of ABC transporters (Zoghbi and Altenberg, 2014).

No difference in binding pocket size was observed between active and inactive systems, consistent with previous findings in simulations without ATP. Inactive compounds were unable to induce variations in the pocket size, and the presence of ATP did not impact this aspect.

Additionally, structural changes associated with the transport mechanism were evident in the SASA results. In the presence of ATP, residues in the extracellular loop and certain intracellular loops in TM4 and TM10 showed increased SASA values, indicating their correlation

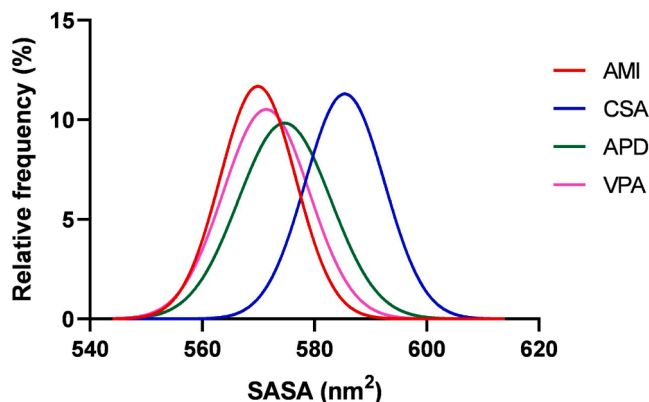


Fig. 9. Distributions of the total solvent-accessible surface area (SASA) for the studied systems.

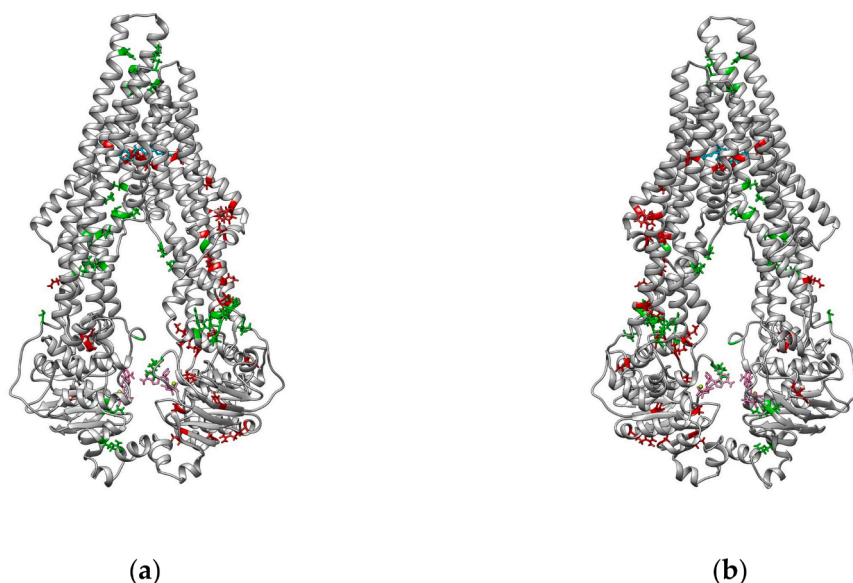


Fig. 10. P-Glycoprotein residues with significant Solvent-Accessible Surface Area (SASA) variations: (a) Frontal view; (b) Rear view. Residues highlighted in red indicate smaller SASA values in active systems. Residues highlighted in green indicate larger SASA values in active systems.

with the characteristic movement at the onset of the transport mechanism.

In essence, this work provides clear evidence that the onset of the translocation pathway is triggered by a ligand occupying the binding pocket, with NBD1 playing a pivotal role. Recent studies (Murakami et al., 2023) have also explored the correlation between NBD1 flexibility and transport mechanism. Furthermore, the results of this work support the hypothesis of the sandwich dimer conformation for ATP binding.

In general, molecular dynamics has proven to be a valuable tool in gaining comprehensive insights into P-gp's interactions with diverse ligands. These results hold relevance not only in drug development but also in the field of toxicity assessment as this information is crucial for understanding the energy-driven transport mechanism.

Institutional Review Board Statement

Not applicable.

Funding

The work was funded by the Marie Skłodowska-Curie Action-Innovative Training Network project in3, under grant no. 721975 and the Slovenian Research Agency; ARIS program grant P1-0017.

CRedit authorship contribution statement

Novic Marjana: Writing – review & editing, Supervision, Project administration, Funding acquisition. **Pérez-Castillo Yuniorkis:** Writing – review & editing, Supervision, Methodology, Investigation, Formal analysis, Conceptualization. **Mora Lagares Liadys:** Writing – original draft, Validation, Methodology, Investigation, Conceptualization.

Declaration of Competing Interest

The authors declare that they have no known competing financial interests or personal relationships that could have appeared to influence the work reported in this paper.

Data Availability

Data will be made available on request.

Appendix A. Supporting information

Supplementary data associated with this article can be found in the online version at doi:10.1016/j.tox.2024.153732.

References

- Alam, A., et al., 2019. Structural insight into substrate and inhibitor discrimination by human P-glycoprotein. *Science* 363 (6428), 753–756. <https://doi.org/10.1126/science.aav7102>.
- Ambudkar, S.V., et al., 2003. P-glycoprotein: from genomics to mechanism. *Oncogene* 22 (47), 7468–7485. <https://doi.org/10.1038/sj.onc.1206948>.
- Bakan, A., Meireles, L.M., Bahar, I., 2011. ProDy: protein dynamics inferred from theory and experiments. *Bioinformatics* 27 (11), 1575–1577. <https://doi.org/10.1093/bioinformatics/btr168>.
- Baltes, S., et al., 2007. Valproic acid is not a substrate for P-glycoprotein or multidrug resistance proteins 1 and 2 in a number of in vitro and in vivo transport assays. *J. Pharmacol. Exp. Ther.* 320 (1), 331–343. <https://doi.org/10.1124/jpet.106.102491>.
- Case, D.A., I.Y.B.-S., Brozell, S.R., Cerutti, D.S., Cheatham III, T.E., Cruzeiro, V.W.D., Darden, T.A., et al., 2018. *AMBER*. University of California, San Francisco, CA.
- Chen, J., et al., 2003. A tweezers-like motion of the ATP-binding cassette dimer in an ABC transport cycle. *Mol. Cell* 12 (3), 651–661.
- Condic-Jurkic, K., et al., 2018. The reliability of molecular dynamics simulations of the multidrug transporter P-glycoprotein in a membrane environment. *PLoS One* 13 (1), e0191882. <https://doi.org/10.1371/journal.pone.0191882>.
- Dehghani-Ghahnaviyeh, S., Kapoor, K., Tajkhorshid, E., 2021. Conformational changes in the nucleotide-binding domains of P-glycoprotein induced by ATP hydrolysis. *FEBS Lett.* 595 (6), 735–749. <https://doi.org/10.1002/1873-3468.13992>.
- Domicieva, L., Biggin, P.C., 2015. Homology modelling of human P-glycoprotein. *Biochem. Soc. Trans.* 43 (5), 952–958. <https://doi.org/10.1042/BST20150125>.
- Eyal, S., et al., 2006. The antiepileptic and anticancer agent, valproic acid, induces P-glycoprotein in human tumour cell lines and in rat liver. *Br. J. Pharmacol.* 149 (3), 250–260. <https://doi.org/10.1038/sj.bjp.0706830>.
- Ferreira, R., Ferreira, M.-J.U., Dos Santos, D.J., 2012. Insights on P-glycoprotein's efflux mechanism obtained by molecular dynamics simulations. *J. Chem. Theory Comput.* 8 (6), 1853–1864. <https://doi.org/10.1021/ct300083m>.
- Grigoreva, T.A., et al., 2022. Analysis of P-glycoprotein transport cycle reveals a new way to identify efflux inhibitors. *ACS Omega* 7 (47), 42835–42844. <https://doi.org/10.1021/acsomega.2c04768>.
- He, X., et al., 2020. A fast and high-quality charge model for the next generation general AMBER force field. *J. Chem. Phys.* 153 (11) <https://doi.org/10.1063/5.0019056>.
- Humphrey, W., Dalke, A., Schulten, K., 1996. VMD: visual molecular dynamics. *J. Mol. Graph.* 14 (1), 33–38. [https://doi.org/10.1016/0263-7855\(96\)00018-5](https://doi.org/10.1016/0263-7855(96)00018-5).
- Jin, M.S., et al., 2012. Crystal structure of the multidrug transporter P-glycoprotein from *Caenorhabditis elegans*. *Nature* 490 (7421), 566–569. <https://doi.org/10.1038/nature11448>.
- Jo, S., et al., 2014. CHARMM-GUI PDB manipulator for advanced modeling and simulations of proteins containing nonstandard residues. *Adv. Protein Chem. Struct. Biol.* 96, 235–265. <https://doi.org/10.1016/bs.apcsb.2014.06.002>.
- Jo, S., et al., 2008. CHARMM-GUI: a web-based graphical user interface for CHARMM. *J. Comput. Chem.* 29 (11), 1859–1865. <https://doi.org/10.1002/jcc.20945>.

- Jones, P.M., George, A.M., 1999. Subunit interactions in ABC transporters: towards a functional architecture. *FEMS Microbiol. Lett.* 179 (2), 187–202. <https://doi.org/10.1111/j.1574-6968.1999.tb08727.x>.
- Jones, P.M., George, A.M., 2002. Mechanism of ABC transporters: a molecular dynamics simulation of a well characterized nucleotide-binding subunit. *Proc. Natl. Acad. Sci.* 99 (20), 12639–12644. <https://doi.org/10.1073/pnas.152439599>.
- Jouan, E., et al., 2016. Evaluation of P-glycoprotein inhibitory potential using a rhodamine 123 accumulation assay. *Pharmaceutics* 8 (2), 12. <https://doi.org/10.3390/pharmaceutics8020012>.
- Juliano, R.L., Ling, V., 1976. A surface glycoprotein modulating drug permeability in Chinese hamster ovary cell mutants. *Biochim. Et. Biophys. Acta (BBA)-Biomembr.* 455 (1), 152–162. [https://doi.org/10.1016/0005-2736\(76\)90160-7](https://doi.org/10.1016/0005-2736(76)90160-7).
- Kim, Y., Chen, J., 2018. Molecular structure of human P-glycoprotein in the ATP-bound, outward-facing conformation. *Science* 359 (6378), 915–919. <https://doi.org/10.1126/science.aar7389>.
- Kodan, A., et al., 2014. Structural basis for gating mechanisms of a eukaryotic P-glycoprotein homolog. *Proc. Natl. Acad. Sci.* 111 (11), 4049–4054. <https://doi.org/10.1073/pnas.1321562111>.
- Lee, J., et al., 2020. CHARMM-GUI supports the Amber force fields. *J. Chem. Phys.* 153 (3), 035103 <https://doi.org/10.1063/5.0012280>.
- Leslie, E.M., Deeley, R.G., Cole, S.P., 2005. Multidrug resistance proteins: role of P-glycoprotein, MRP1, MRP2, and BCRP (ABCG2) in tissue defense. *Toxicol. Appl. Pharmacol.* 204 (3), 216–237. <https://doi.org/10.1016/j.taap.2004.10.012>.
- Li, Y., et al., 2010. The structure and functions of P-glycoprotein. *Curr. Med. Chem.* 17 (8), 786–800. <https://doi.org/10.2174/092986710790514507>.
- Li, D., et al., 2014. ADMET evaluation in drug discovery. 13. Development of in silico prediction models for P-glycoprotein substrates. *Mol. Pharm.* 11 (3), 716–726. <https://doi.org/10.1021/mp400450m>.
- Lusvarghi, S., Ambudkar, S.V., 2019. ATP-dependent thermostabilization of human P-glycoprotein (ABCB1) is blocked by modulators. *Biochem. J.* 476 (24), 3737–3750. <https://doi.org/10.1042/BCJ20190736>.
- McGibbon, R.T., et al., 2015. MDTraj: a modern open library for the analysis of molecular dynamics trajectories. *Biophys. J.* 109 (8), 1528–1532. <https://doi.org/10.1016/j.bpj.2015.08.015>.
- Mora Lagares, L., et al., 2021. Structure–function relationships in the human P-glycoprotein (ABCB1): insights from molecular dynamics simulations. *Int. J. Mol. Sci.* 23 (1), 362. <https://doi.org/10.3390/ijms23010362>.
- Mora Lagares, L., et al., 2020. Homology modeling of the human P-glycoprotein (ABCB1) and insights into ligand binding through molecular docking studies. *Int. J. Mol. Sci.* 21 (11), 4058. <https://doi.org/10.3390/ijms21114058>.
- Murakami, M., et al., 2023. Second-site suppressor mutations reveal connection between the drug-binding pocket and nucleotide-binding domain 1 of human P-glycoprotein (ABCB1). *Drug Resist. Updates*, 101009. <https://doi.org/10.1016/j.drup.2023.101009>.
- O'Mara, M.L., Mark, A.E., 2012. The effect of environment on the structure of a membrane protein: P-glycoprotein under physiological conditions. *J. Chem. Theory Comput.* 8 (10), 3964–3976. <https://doi.org/10.1021/ct300254y>.
- Pan, L., Aller, S.G., 2015. Equilibrated atomic models of outward-facing P-glycoprotein and effect of ATP binding on structural dynamics. *Sci. Rep.* 5 (1), 7880 <https://doi.org/10.1038/srep07880>.
- Petersen, E.F., et al., 2004. UCSF Chimera—a visualization system for exploratory research and analysis. *J. Comput. Chem.* 25 (13), 1605–1612. <https://doi.org/10.1002/jcc.20084>.
- Roe, D.R., Cheatham III, T.E., PTRAJ, CPPTRAJ, 2013. Software for processing and analysis of molecular dynamics trajectory data. *J. Chem. Theory Comput.* 9 (7), 3084–3095. <https://doi.org/10.1021/ct400341p>.
- Saeki, T., et al., 1993. Human P-glycoprotein transports cyclosporin A and FK506. *J. Biol. Chem.* 268 (9), 6077–6080. [https://doi.org/10.1016/S0021-9258\(18\)53221-X](https://doi.org/10.1016/S0021-9258(18)53221-X).
- Schmeisser, S., et al., 2023. New approach methodologies in human regulatory toxicology – Not if, but how and when! *Environ. Int.* 178, 108082 <https://doi.org/10.1016/j.envint.2023.108082>.
- Sharom, F.J., 2008. ABC multidrug transporters: structure, function and role in chemoresistance. *Pharmacogenomics* 9 (1). <https://doi.org/10.2217/14622416.9.1.105>.
- Smith, P.C., et al., 2002. ATP binding to the motor domain from an ABC transporter drives formation of a nucleotide sandwich dimer. *Mol. Cell* 10 (1), 139–149. [https://doi.org/10.1016/S1097-2765\(02\)00576-2](https://doi.org/10.1016/S1097-2765(02)00576-2).
- Wagner, J.R., et al., 2017. POVME 3.0: software for mapping binding pocket flexibility. *J. Chem. Theory Comput.* 13 (9), 4584–4592. <https://doi.org/10.1021/acs.jctc.7b00500>.
- Weiser, J., Shenkin, P.S., Still, W.C., 1999. Approximate atomic surfaces from linear combinations of pairwise overlaps (LCPO). *J. Comput. Chem.* 20 (2), 217–230. [https://doi.org/10.1002/\(SICI\)1096-987X\(19990130\)20:2<217::AID-JCC4>3.0.CO;2-A](https://doi.org/10.1002/(SICI)1096-987X(19990130)20:2<217::AID-JCC4>3.0.CO;2-A).
- Wigler, P.W., 1999. PSC833, cyclosporinA, and dextrin/glycine effects on cellular calcein retention and inhibition of the multidrug resistance pump in human leukemic lymphoblasts. *Biochem. Biophys. Res. Commun.* 257 (2), 410–413. <https://doi.org/10.1006/bbrc.1999.0475>.
- Yang, H.-w., et al., 2008. Increased P-glycoprotein function and level after long-term exposure of four antiepileptic drugs to rat brain microvascular endothelial cells in vitro. *Neurosci. Lett.* 434 (3), 299–303. <https://doi.org/10.1016/j.neulet.2008.01.071>.
- Zhang, B., et al., 2021. Simultaneous binding mechanism of multiple substrates for multidrug resistance transporter P-glycoprotein. *Phys. Chem. Chem. Phys.* 23 (8), 4530–4543. <https://doi.org/10.1039/D0CP05910B>.
- Zhou, S.-F., 2008. Structure, function and regulation of P-glycoprotein and its clinical relevance in drug disposition. *Xenobiotica* 38 (7–8), 802–832. <https://doi.org/10.1080/00498250701867889>.
- Zoghbi, M.E., Altenberg, G.A., 2014. ATP binding to two sites is necessary for dimerization of nucleotide-binding domains of ABC proteins. *Biochem. Biophys. Res. Commun.* 443 (1), 97–102. <https://doi.org/10.1016/j.bbrc.2013.11.050>.